GSA Data Repository Item 2017143
Johnstone, S.A., Chadwick, K.D., Frias, M., Tagliaro, G., and Hilley, G.E., 2017, Soil development over mud-rich rocks produces landscape-scale erosional instabilities in the northern Gabilan Mesa, California: GSA Bulletin, doi:10.1130/B31546.1.

IMPACT OF ARROYO EXPANSION ON DRAINAGE DENSITY

Geomorphic mapping within the Wildhorse Valley reveals what appears to be a high concentration of drainages within arroyos (Fig. DR1). Here we formally assess this observation and explore the implications.

Methods

We characterize the extent and locations of the drainage network manually (Fig. DR1). In larger channels, banks defining the bounds of channels were directly identified from shaded topography. This could be accomplished for some deeply incised headwater channels, but channel banks were not always identifiable in 1-m elevation data. We extended channel networks along regions where curvatures are strongly concave (e.g., ~0.1 m^{-1} or greater) along elongate bands no more than a few meters wide. Within each of the tributary basins (Fig. 3 and DR1) defined by our automated procedure we measure drainage density (cumulative channel length divided by watershed area) and relate this to the fraction of those drainage basins occupied by arroyos (Fig. DR2).

We evaluate the significance of correlations between measurements using the larger of two *p*-values determined from the non-parametric Spearman's rank test and with linear regressions, where we assess the significance of the slope of the correlation. We assigned significance when $p < 0.001$.

Results and Discussion

The drainage density measured in the Wildhorse Valley is 4.2 km^{-1}, and is distributed disproportionately among north- and south-flowing tributary basins. Within north-flowing tributaries drainage density varies from 0 to 7.3 km^{-1}, with a median value of 2.2 km^{-1}. This distribution is significantly different ($p_{max} = 1 \times 10^{-10}$) than that of south-flowing tributary basins, whose drainage density ranges from 0 to 13.4 km^{-1}, with a median of 5.5 km^{-1} (Fig. DR2A). Across all drainage basins, drainage density increases with the fraction of these basins occupied by arroyos. The best-fitting linear regression to drainage density data as a function of the fraction of a basin occupied by arroyos gives an intercept of 2.5 ± 0.5 and a slope of 19.5 ± 3.2 ($p = 8 \times 10^{-21}$ and 3×10^{-22}, respectively).

Our mapping highlights that the drainage density within tributaries increases with the fraction of those tributaries occupied by arroyos (Fig. DR2B). The total drainage density of a drainage basin containing arroyos and soil mantled regions can be cast as a sum of the contributors to drainage density:

$$1. D_t = (Ls + Lb + La)/Ac \ .$$

Here D [L^{-1}] is drainage density and the subscript t denotes the total drainage density of a basin. This is given by the sum of the lengths of soil mantled channels, L_s [L]; the lengths of bifurcations within arroyos, L_b [L]; and the length of the longest channel within the arroyo, L_a

[L], divided by the catchment area, A_c [L^2]. By approximating the area of an arroyo as a rectangle of length L_a and width w [L], and converting the ratio of component lengths to the drainage density within those components by accounting for the fraction of the basin occupied by arroyos, f [], the respective drainage densities and arroyo geometry are related as:

$$2. D_t = D_s + (D_b + 1/w - D_s)f.$$

Where the subscripts *s* and *b* denote drainage densities in soil-mantled terrain and due to bifurcations within arroyos, respectively. The drainage density due to arroyo bifurcations is the difference between the total drainage density within arroyos and the drainage density of arroyos from the longest channel, $1/w$. We measure D_s as the drainage density in basins without arroyos where channels were mapped (i.e., $f = 0$), which have a mean drainage density of 2.8 km^{-1} (standard deviation, 1.5 km^{-1}). Within arroyos, which are typically ~75 m wide, we measure a mean drainage density of 28.9 km^{-1} (standard deviation 14.7 km^{-1}). In the context of Equation 2 this gives a D_b of ~15 km^{-1}. The similarity between D_b and $1/w$ suggests that the addition of channels within the bedrock and scree walls of arroyos effectively doubles the drainage density within these features. In the framework of Equation 2 the best fitting linear regression to D_t data as a function of f (Fig. DR2) yields a D_s of 2.5 ± 0.5 km^{-1} and a value of 22.0 ± 3.2 km^{-1} for the sum of D_b and $1/w$, within the range of observations for these parameters obtained above. Therefore, increases in drainage density above that observed in soil mantled catchments (Fig. DR2) should reflect a combination of the lengthening of mainstem channels by headward expansion of arroyos and the addition of channel segments within arroyos.

EVIDENCE OF LATERAL CHANNEL MIGRATION IN THE WILDHORSE VALLEY

Past work in the Gabilan Mesa suggested that relatively high sediment loads were delivered to mainstem valleys from south flowing tributaries, and preferentially deflected streams to the south (Dohrenwend, 1978). Over time such a southward migration of trunk channels was believed to give rise to the observed asymmetry in the size of north- and south-flowing drainages. Using our geomorphic mapping and topographic analysis we highlight evidence in support of the basic tenants of this lateral migration hypothesis, although these findings do not predict how much of the observed asymmetry has resulted from lateral migration.

Methods

We measured the density of fans within mainstem valleys and determined the mean downslope direction of these features to estimate relative differences in the flux of sediment delivered to mainstem valleys from north and south flowing tributaries. Fan density is calculated as the ratio of the fan areas within a search window to the area of all terrace surfaces and fans within that search window. We calculated independent fan densities for fans whose orientations place them in different aspect classes. Individual fans were assigned an aspect based on the orientation of the slope vector determined from the coefficients of the best-fitting plane computed from the 1-m elevation data contained within fan boundaries. We defined 26 search windows by first constructing lines that traverse mainstem valleys where a single valley floor deposit is present and extensive (Fig. DR1). We segmented these lines into portions that are slightly longer than one valley width (~300 m), and buffered them to create rectangular search windows 600 m wide.

We collected two sets of swath profiles across valley surfaces in ALSM data using a swath radius of 2 m to highlight how variations in sediment flux have influenced valley morphology. In the first set, 'cross valley profiles', locations of swath profiles across valley surfaces were selected to be roughly perpendicular to the trend of valleys, to have orientations within 45° of N-S, and to traverse valleys at locations away from tributary mouths (Fig. DR1). Additionally, we trimmed this first set of profiles to show 20 m of relief. In the second set of swath profiles, 'fan-traversing profiles', we targeted locations of confluences between tributaries and mainstem valleys. These profiles were oriented approximately perpendicular to the mainstem valleys and were not restricted to any particular orientation. Profiles originated or were terminated either at the limit of mapped valley-fill surfaces or at the approximate location of the projection of this limit to the midpoint of tributary mouths (Fig. DR1).

Using fan-traversing profiles we compared the asymmetry in fan length on either side of valleys to the valley floor asymmetry. Fan length asymmetry is measured as the difference between the length of fans derived from the left of the profile (looking upstream), $L_{f(l)}$, and the right of the profile, $L_{f(r)}$, divided by the total length of the profile, L_t. We measured valley asymmetry using the ratio of the distance to the lowest elevation point from the left end of the valley profile, L_{thal}, to L_t. We subtracted ½ from the valley asymmetry and divided the fan length asymmetry by 2 so that both quantities may vary from -½ to ½, such that the axial location of a channel within a symmetric valley would be located at 0.

We evaluate the significance of correlations between measurements using the larger of two *p*-values determined from the non-parametric Spearman's rank test and with linear regressions, where we assess the significance of the slope of the correlation. We assigned significance when $p < 0.001$.

Results and Discussion

The density of fans in any aspect class varies between 0.09 and 1, with a median value of 0.6. North-flowing fans make up 0%–60% of valley floor deposits (median: 2%), while south-flowing fans occupy between 9% and 100% of valley floor deposits (median: 47%). The distributions of these fan densities are distinct from one another ($p_{max} = 9 \times 10^{-8}$, Fig. DR3B). Qualitatively, cross-valley profiles highlight that main-stem channels are typically offset toward the south side of valleys (Fig. DR3A). Mainstem channels often abut north-facing hillslopes, but are separated from the toes of south-facing hillslopes by a steady, south-directed slope. Asymmetry in the position of the thalweg within mainstem valleys is positively correlated with asymmetry in the length of fans sourced from either side of these valleys ($p_{max} = 3.8 \times 10^{-6}$). The predominance of south flowing fans and the bias of channels toward the south sides of mainstem valleys are recorded by the clustering of data within the upper right quadrant of Fig. DR3C.

Near the upstream limit of incision by the Q_{tsy} surface, the Q_{tso} surface is a fill terrace, and so the fans sourced from tributary catchments probably facilitated a component of aggradation and valley filling (e.g., García and Mahan, 2009). However, without differential subsidence across the valley or preferential fan erosion, the areal extent of these fans provides constraints on the relative sediment delivery from north- versus south-flowing tributaries. South-flowing fans occupy a larger fraction of mainstem valleys than north-flowing fans (Fig. DR3). Differences in the extent of fans suggest that more sediment is being delivered from south-facing aspects, consistent with the fact that south-flowing drainages are generally larger and may be expanding headward. While nearly all south-flowing tributaries have fans at the intersection of

mainstem valleys, the same is not true for north flowing tributaries (Fig. DR1). Either north-flowing fans are preferentially removed from these valleys, the events that construct fans are less frequent in north-flowing tributaries, or a combination of these mechanisms is at play. Along these lines, the much larger colluvial hollows present in north-flowing drainage basins indicate that these catchments may not flush the sediment trapped within hollows with the same frequency as south flowing catchments (Fig. 8). At timescales shorter than that of hollow excavation and filling, which may be related to cyclicity in climate (Reneau et al., 1986), this may also lead to a reduced sediment flux from north flowing drainages.

The Q_{tso} surface shows a southward cross-valley slope. Asymmetry in the position of the channel within this surface correlates with asymmetry in the extent of fans sourced from either side of mainstem valleys. Thus, it appears that the aspect-controlled asymmetry in sediment supply likely impacts the slope of the major valleys as well (Fig. DR3). This may lead to the cross-valley migration of the major channels during accumulation of the Q_{tso} surface, which might have the effect of truncating north-facing hillslopes (Dohrenwend, 1978). Near the outlet of the Wildhorse Valley the extensive and exclusive preservation of the Q_{tso} surface along the north side of the modern channel is consistent with the southward migration of channels in these large alluviated valleys (Fig DR1).

REFERENCES CITED

Dohrenwend, J.C., 1978, Systematic valley asymmetry in the central California Coast Ranges: Geological Society of America Bulletin, v. 89, no. 6, p. 891, doi:10.1130/0016-7606(1978)89<891:SVAITC>2.0.CO;2.

García, A.F., and Mahan, S.A., 2009, Sediment storage and transport in Pancho Rico Valley during and after the Pleistocene-Holocene transition, Coast Ranges of central California (Monterey County): Earth Surface Processes and Landforms, v. 34, no. 8, p. 1136–1150, doi:10.1002/esp.1804.

Reneau, S.L., Dietrich, W.E., Dorn, R.I., Berger, C.R., and Rubin, M., 1986, Geomorphic and paleoclimatic implications of latest Pleistocene radiocarbon dates from colluvium-mantled hollows, California: Geology, v. 14, no. 8, p. 655, doi:10.1130/0091-7613(1986)14<655:GAPIOL>2.0.CO;2.

FIGURE CAPTIONS

Figure DR1. Full geomorphic map of the Wildhorse Valley. Colored polygons denote different geomorphic process domains. Small rectangles indicate the location of detailed maps of arroyos shown in Figure 4. Lines across and along valleys in the upper part of the catchment were used to produce Fig. DR3. Tributary basins bound by red, black, and green dashed lines were used to calculate basin specific calculations (e.g., Fig. 8). Labeled arrows highlight significant features discussed in the text.

Figure DR2. Drainage density within the Wildhorse Valley. (A) Boxplots of drainage density within north-flowing, south-flowing, and other tributaries. Extent of catchments is shown in Figure 3. Dashed line shows the drainage density measured on the whole of the Wildhorse Valley. (B) Relationship between the fraction of a basin occupied by arroyos, f (Fig. 8), and the drainage density of that basin. Dashed lines show the uncertainty associated with the regression coefficients.

Figure DR3. (A) Cross valley profiles are smoothed swath profiles, the locations of profiles are shown in Fig. DR1. (B) Box plots of fan density in different aspect classes in the upper portions of the Wildhorse Valley (see text for details). Dashed line shows the median density of fans in any aspect class. (C) Plots of the asymmetry in the thalweg position (e.g., the 0 position in A) against asymmetry in the length of fans draining from the left and right side ($L_{f(l)}$ and $L_{f(r)}$, respectively) of valleys (facing upstream).

Fig. SF1, Geomorphic map of the Wildhorse Valley

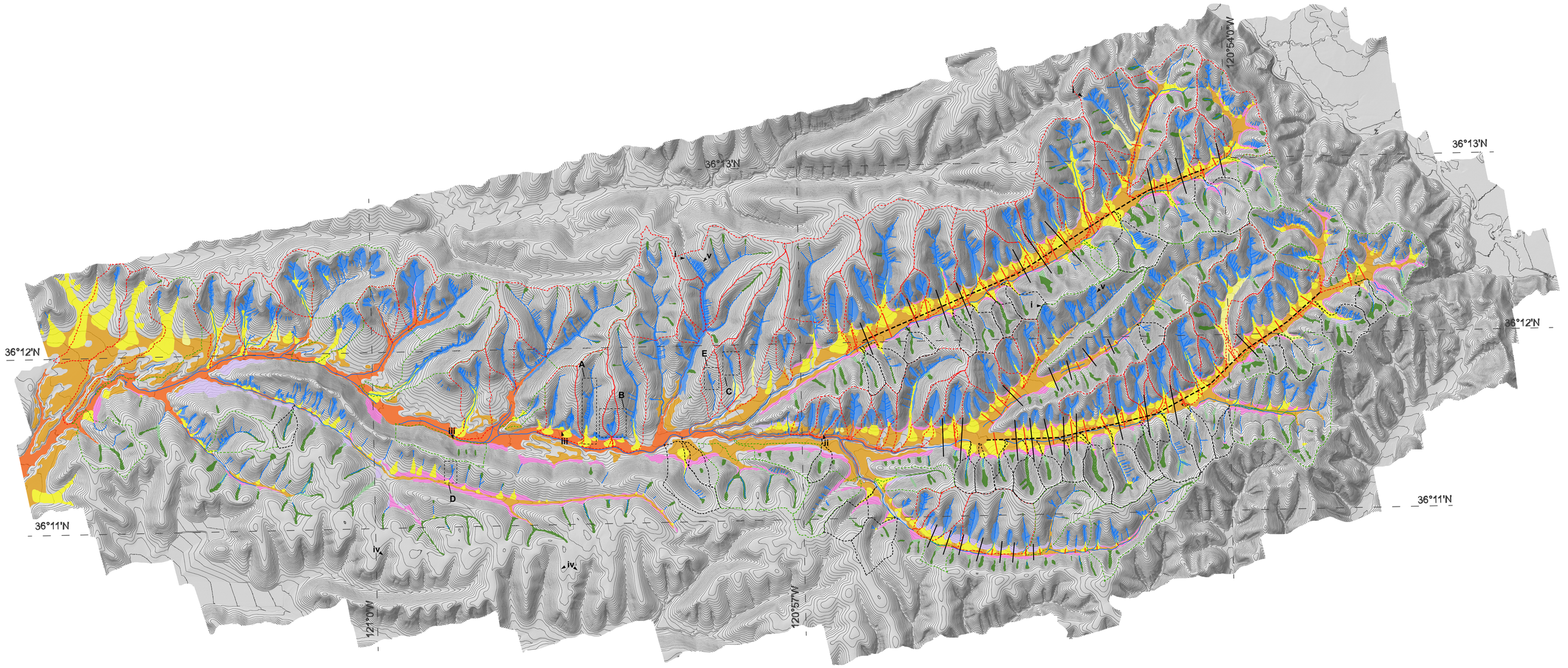

N

1,000 meters

- Arroyo
- Colluvial Hollows (uncertain)
- Colluvial Hollows
- Toe slope apron
- Toe slope apron (uncertain)
- Fan
- Fan (uncertain)
- Qtsy
- Qtso
- Channels
- 5m Contour
- Cross valley fan profiles
- Cross valley profiles
- Along Valley lines
- Location of detailed maps
- North flowing drainage basins analyzed
- South flowing drainage basins analyzed
- East/west flowing drainage basins analyzed

- Feature/ relationship discussed in text
- **i** Arroyo breaching drainage divide
- **ii** Arroyo margins continuous with incised terrace surface
- **iii** Lateral erosion into north and south facing slopes
- **iv** South flowing tributaries penetrating mesa surface
- **v** High drainage density within arroyo

Fig. SF2, Drainage density

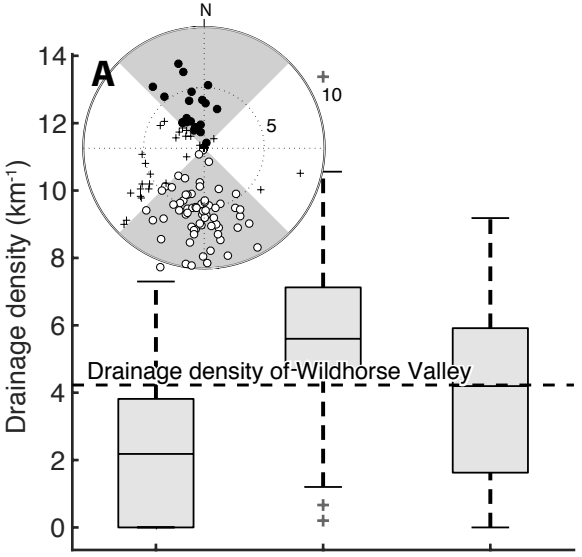

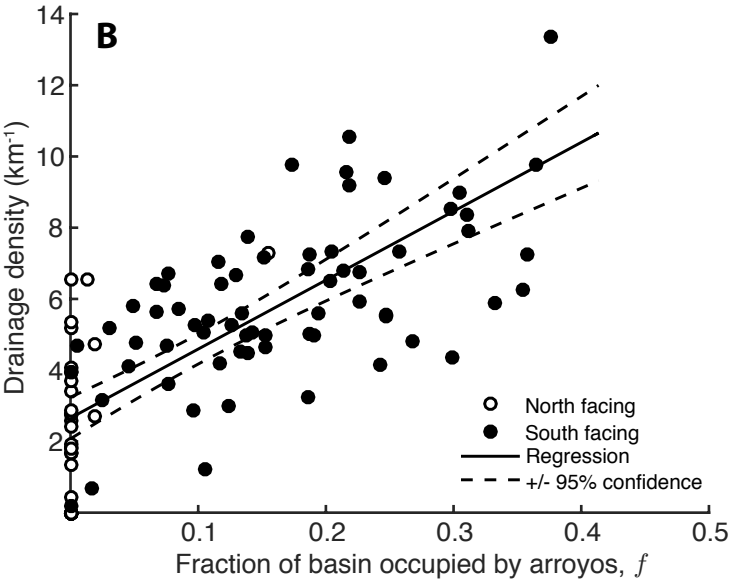

Fig. SF3, Valley morphology